Available online at www.sciencedirect.com

ScienceDirect

Ceramics International 41 (2015) 3549–3554

CERAMICS INTERNATIONAL

www.elsevier.com/locate/ceramint

Crystal growth and photoluminescence of europium-doped strontium titanate prepared by a microwave hydrothermal method

R.F. Gonçalves[a,*], A.P. Moura[c], M.J. Godinho[b,c], E. Longo[c], M.A.C. Machado[c,e], D.A. de Castro[b], M. Siu Li[d], A.P.A. Marques[a]

[a]UNIFESP-Universidade Federal de São Paulo, Rua Prof. Artur Riedel, 275, Diadema, SP, CEP 09972-270, Brazil
[b]UFG-Universidade Federal de Goiás, Departamento de Química-CAC, 75.704– 020, Catalão, GO, Brazil
[c]LIEC-IQ-Universidade Estadual Paulista, P.O. Box 355, 14801-907, Araraquara, SP, Brazil
[d]IFSC-Universidade de São Paulo, P.O. Box 369, 13560 970, São Carlos, SP, Brazil
[e]UFPA-Universidade Federal do Pará, Faculdade de Física, Rua Augusto Corrêa, 01, Belém, PA, CEP 66075-110, Brazil

Received 7 October 2014; received in revised form 31 October 2014; accepted 2 November 2014
Available online 13 November 2014

Abstract

This article reports that europium-doped strontium titanate ($SrTiO_3$:Eu^{3+}) was successfully synthesized using a co-precipitation method at room temperature with processing in a microwave-hydrothermal system at 140 °C for 30 min. Phase composition and structure were examined using X-Ray Diffraction, and Fourier-Transform Raman spectroscopy, revealing a cubic structure with a *Pm3m* space group. The optical properties were investigated by ultraviolet-visible absorption and photoluminescence, which showed that red emissions originate from Eu^{3+} transitions. Field emission scanning electron microscopy revealed spherical-like Eu^{3+} doped $SrTiO_3$ nanoparticles.

Keywords: $SrTiO_3$; Nanocrystals; Europium; Photoluminescence

1. Introduction

$SrTiO_3$ compounds are members of an important inorganic materials family with a distinctive perovskite-type structure and have been investigated because of their unique structure, good chemical and physical stability, strong visible luminescence, and excellent optical properties [1,2]. Such characteristics can be used in applications, such as optoelectronic devices, gas sensors, photocatalysts, or photoelectrodes, to improve efficiency [3,4]. Moreover, structural changes can result in $SrTiO_3$ having diverse physical and chemical properties. Some new optical properties of this material can be obtained by doping it with rare earth (RE) ions [5,6]. Nanoparticles of inorganic compounds activated by RE ions have received much attention due to their broad applicability and potential use in technology [7,8]. New matrices are desperately needed for doping to enrich the categories of products and develop a more common and comprehensive theory [9]. Eu^{3+} ions are important because of their potential application as red phosphors, in optical amplifiers, in electroluminescent devices, and in lasers [10,11]. Among all the RE ions, Eu^{3+} is usually employed as a red emitting center because of its unique $4f^6$ configuration that can be effectively activated by ultraviolet rays or cathode rays and emits high purity red light [12].

Preparation techniques that have been proposed to fabricate $SrTiO_3$ include solid-state reaction procedures [13] and polymeric precursor methods [14]. However, these synthesis routes result in agglomeration of particles and require a high synthesis temperature and large amounts of energy. In addition, they produce a poor morphology of phosphor particles and an uneven distribution of particle size at a low production rate with long preparation cycles. Consequently, it is very important to develop economic and simple synthesis methods for titanate materials. The microwave hydrothermal (MH) method has drawn tremendous attention owing to its

*Corresponding author. Fax +55 16 3351 8214.
E-mail address: rosanaf.gon@gmail.com (R.F. Gonçalves).

http://dx.doi.org/10.1016/j.ceramint.2014.11.018
0272-8842/

advantages, such as low reaction temperature, energy economy, well-defined product morphology, and energy efficiency, because power is only applied within the reactive mixture. The microwave-assisted processing is fast, clean, simple, and often more energetically efficient than conventional heating [15,16].

This article reports a successful synthesis of $SrTiO_3$ doped with 1 mol% of Eu^{3+} crystal phosphors by the MH method. $SrTiO_3$ was chosen as the host, because it has attractive chemical and thermal stability properties.

2. Experimental details

2.1. Synthesis and MH processing of $SrTiO_3$:Eu crystals

$SrTiO_3$ doped with 1 mol% of Eu^{3+} powders were synthesized by co-precipitation without surfactants in aqueous solutions. $Ti(OC_3H_7)_4$ (99.99%, Aldrich), $SrCl_2.2H_2O$ (99.9%, Merck), and KOH (99%, Merck) were used as starting materials. First, 0.01 mol of $Ti(OC_3H_7)_4$ was slowly added to 25 mL of deionized water while stirring. Similarly, 0.01 mol of $SrCl_2.2H_2O$ was dissolved in 25 mL of deionized water, separately, with constant stirring. $Eu(NO_3)_3 \cdot 5H_2O$ (1 mol% Eu^{3+} with respect to Sr^{2+}, 99.99%, Aldrich) was added to this reaction mixture. KOH was used as a mineralizer agent. The mixture containing all the ions was transferred to a Teflon autoclave with 100 mL capacity (80% filled), sealed, and placed in the MH system using 2.45- GHz microwave radiation with a maximum power of 800 W. The reactional mixture was heated at 140 °C for 30 min. This was followed by natural cooling of the autoclave to room temperature. The product was washed several times until a neutral pH was obtained and dried at 70 °C for 6 h.

2.2. Characterization of $SrTiO_3$:Eu^{3+} crystals

The obtained crystals were structurally characterized from X-ray powder diffraction (XRD) patterns using a Shimadzu-XRD-6000 (Japan) with Cu-Kα radiation (λ=1.5406 Å) in the 2θ range from 10° to 70° with a scanning velocity of 2°/min in normal routine scanning. FT-Raman spectroscopy was performed with a Bruker-RFS 100 (Germany). The Raman spectra were obtained using a 1064-nm line with a Nd:YAG laser, while keeping its maximum output power at 100 mW, in the range from 50 to 1000 cm^{-1}. The morphologies of $SrTiO_3$:Eu^{3+} crystals were observed by field emission scanning electron microscopy (FE-SEM) through a Carl Zeiss, model Supra 35-VP (Germany) operated at 6 kV. Ultraviolet-visible (UV-vis) diffuse reflectance spectra were produced using a Varian spectrophotometer model Cary 5G (USA) in diffuse reflectance mode. Photoluminescence (PL) measurements were performed using a Jobin Yvon-Fluorolog spectrofluorometer under continuous Xe lamp (450 W) excitation at room temperature (λ=393 nm).

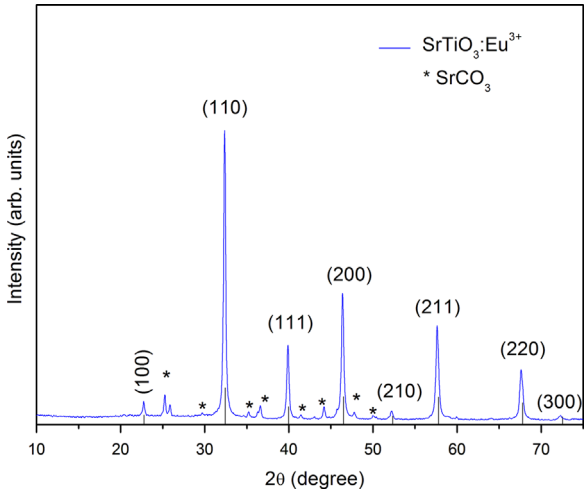

Fig. 1. XRD patterns of $SrTiO_3$: Eu^{3+} processed in a microwave-assisted hydrothermal method at 140 °C for 30 min.

3. Results and discussion

3.1. XRD patterns

The XRD patterns of the $SrTiO_3$ obtained by the co-precipitation method and processed in an MH system are shown in Fig. 1. The diffraction peaks match the standard data of a cubic phase with a *Pm3m* space group, according to the Joint Committee for Powder Diffractions Standards, JCPDS Card N° 35-0734 as indicated. Some traces of additional peaks correspond to impurity phases (marked by ✻), which are attributed to the $SrCO_3$ phase and are probably due the existence of strontium vacancies in the $SrTiO_3$ structure. The $SrCO_3$ phase corresponds to the *Pmcn* orthorhombic structure indexed by JCPDS card N° 05-0418.

3.2. FT-Raman spectroscopy analysis

Raman spectroscopy has been used to study the structure and symmetry in solids as well as phase transitions in different perovskites [17]. The phenomenon of inelastic light scattering is generally used to investigate the behavioral changes in the local symmetry of ceramics. Fig. 2 illustrates the Raman spectrum for the sample of $SrTiO_3$:Eu prepared by co-precipitation and processed using an MH method. Six Raman-active modes were observed in the range of 150–1100 cm^{-1} that were assigned to the cubic structure. Assignments of Raman active modes for the europium-doped- $SrTiO_3$ structure are shown in Table 1. The information in the table shows an excellent match between the Raman shift of peaks at 177, 264, 545, 736, 800, and 1069 cm^{-1} and the frequencies of TO2, TO3, TO4, TO, LO4, and $SrCO_3$ phonons, respectively. These results agree with those of Moreira et al. [18] who prepared pure strontium titanate nanospheres. The purpose was to perform a joint experimental analysis and first-principle calculations on MH synthesis of ST nanospheres. According to the XRD analysis, the Raman spectrum (Fig. 2) displays a peak at 1069 cm^{-1} that corresponds to $SrCO_3$. Similar

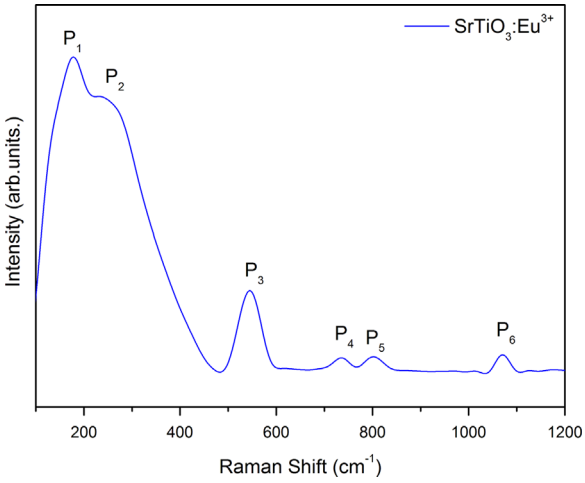

Fig. 2. FT- Raman spectrum of $SrTiO_3$: Eu^{3+}.

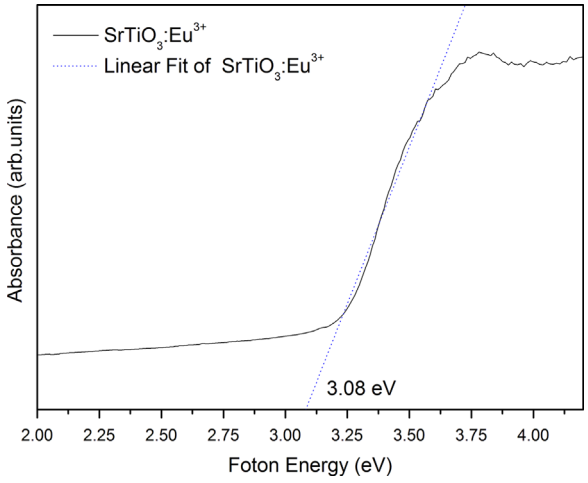

Fig. 3. UV-Vis absorbance spectrum $SrTiO_3$: Eu^{3+}.

Table 1
Frequencies (cm^{-1}) obtained by Raman analysis of $SrTiO_3$:Eu^{3+}.

Vibrational modes		*Ref.* [18]	*ST:Eu*$^{3+}$
TO2 Mode	P_1	179	177
TO3 Mode	P_2	265	264
TO4 Mode	P_3	545	545
TO Mode	P_4	724	736
LO4 Mode	P_5	792	800
$SrCO_3$ Mode	P_6	1072	1069

results have been observed for pure $SrTiO_3$ in other research reported in the literature [19].

3.3. Ultraviolet-visible absorption spectroscopy analysis

The optical band gap (E_g) was calculated by the Wood and Tauc method to understand the effect of structural distortions on the $SrTiO_3$:Eu^{3+} electronic state distribution. In this calculation, the E_g value is related to the absorbance and photon energy. Fig. 3 shows the optical absorbance spectra as a function of photon energy for a sample of strontium titanate doped with 1 mol% of Eu^{3+}.

The absorption curve shows the typical optical behavior of crystalline or structurally arranged materials. A tail with a very subtle absorption gradient is observed after the linear fit forms an angle with the x-axis, which is very close to 90°. The E_{gap} value found by extrapolation of the experimental curve was 3.08 eV for the $SrTiO_3$:Eu sample. E_{gap} values are related to the presence of intermediate levels between the valence band and conduction band due to the presence of a structural disorder-order network of material and are also related to the photoluminescent behavior presented. The reported E_{gap} value for pure strontium titanate (ST) prepared by the polymeric precursor method was approximately 3.2 eV [20]. However, E_{gap} values are very dependent upon the synthesis method, morphology, orientation, and distortions in the lattice, as well as doping [21]. Fig. 3 shows the decrease in the E_{gap} values with respect to the literature value for pure ST as a result of the insertion of Eu^{3+} ions in the $SrTiO_3$ network. This behavior can be related to an increase of intermediary energy levels between the valence band and conduction band. This phenomenon can be explained by new electronic levels related to additional 4*f* orbitals of Eu^{3+} ions. Cavalcante et al. [22] achieved a significant reduction in E_{gap} values (from 4.9 to 3.82 eV) upon the replacement of Ba^{2+} by Pr^{3+} in the $BaWO_4$ lattice. They reported that Pr^{3+} ions induce the appearance of a new intermediary energy level within the optical band gap, since the praseodymium contributes 4*f* orbitals, while the barium exhibits 6 s orbitals in the valence band. These effects were also attributed to distortions in the $BaWO_4$ lattice and the formation of barium and oxygen vacancies. The vacancies are related to the substitution of trivalent Pr^{3+} ions into the A-sites normally occupied by divalent Ba^{2+} ions, which leads to negative charge compensation in the crystal. In other work, Chen et al. [23] explained the correlation between the electronic structure and optical properties of Eu-doped ZnO crystals. According to the authors, when Eu^{3+} ions are incorporated into the ZnO host, they tend to form localized states and introduce electrons (i.e., impurities) into the ZnO band gap, which are responsible for the band gap reduction.

3.4. PL emission analysis

The literature reports that pure strontium titanate displays a broad band spectrum in the range of 400–800 nm with the maximum centered around 460 nm [19]. This broad band luminescence is usually observed in perovskite crystals, associated with the presence of imperfections or defects, and is typical of a multiphonon and multilevel process. In particular, $SrTiO_3$ can accommodate rare-earth ions in the structure; hence, this doping is not only used as a probe to investigate local centers and energy, but also to cause changes in the optical behavior of these materials [24].

Therefore, the presence of Eu^{3+} in the $SrTiO_3$ host results in good luminescence properties. Fig. 4(a) presents the excitation spectrum of the Eu^{3+}-doped $SrTiO_3$ powder,

monitored at the Eu^{3+} emission at 614 nm. In the 350–480 nm spectral range, sharp lines are visible due to the 4*f*-4*f* transitions of the Eu^{3+} ions. The main peak is assigned to the transition of the $^7F_0$ fundamental to the $^5L_0$ excited state at 393 nm.

Fig. 4(b) shows the photoluminescence emission spectrum of the sample of Eu^{3+}-doped $SrTiO_3$ (excited at 393 nm). The ST:Eu^{3+} system has characteristic Eu^{3+} transitions. The peaks are ascribed to the *f*-*f* transitions from the ground state to the excited states of Eu^{3+} ion.

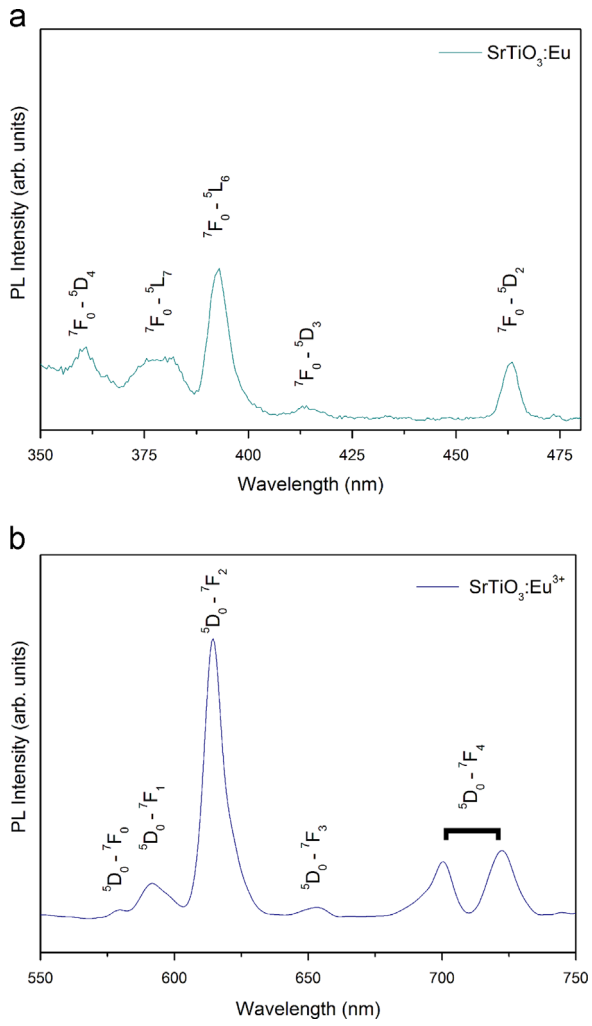

Fig. 4. (a) Excitation spectrum of $SrTiO_3$: Eu^{3+}. (b) Emission spectrum of $SrTiO_3$: Eu^{3+} (λ=393 nm).

The emission spectra for the Eu^{3+} ion presents the most intense emission lines corresponding to the $^5D_0 \rightarrow {}^7F_J$ (J=0,1,2,3,4) transitions and occur in the range of 550–750 nm. The $^5D_0 \rightarrow {}^7F_2$ transition around 614 nm dominates the spectrum and is more intense than the other transitions. Furthermore, the forbidden transition "singlet-singlet" $^5D_0 \rightarrow {}^7F_0$ is detectable and can be seen in the low wavelength region of the spectrum. The $^5D_0 \rightarrow {}^7F_1$ transition results from a forced magnetic dipole mechanism, and its intensity is not significantly altered by perturbation of the crystalline field [25].

In this research, Eu^{3+} replaces Sr^{2+} on the $SrTiO_3$ cubic network and, therefore, charge compensations are required. Defects in the crystal lattice play an important role in the determination of the luminescent properties of the oxides [26,27]. Therefore, direct changing of the contents of some types of defects may cause variations of concentrations of the corresponding luminescence centers [28,29]. In particular, vacancies are very important in the formation of the luminescence-center structure for such crystals [30,31]. Their content may be varied, in particular, by an appropriate doping effect of the material. When the network is excited, the absorbed energy is lost by non-radiative energy transfer due to ion-ion (Eu^{3+}-Eu^{3+}) interactions or ion vacancies (defects generated by the insertion of the dopant into the host matrix). The PL intensity of the ST matrix is reduced while the Eu^{3+} emissions become dominant and are perfectly seen in the spectrum (Fig. 4).

3.5. FE-SEM analysis

The FE-SEM images are shown in Fig. 5 for the $SrTiO_3$: Eu^{3+} compound prepared by an MH method. Beyond the aggregation process, nanoparticles will auto-organize, taking the form of nanospheres. This "self-assembly" process, where the composition is an important element, corresponds to a predefined interaction between individual particles, and results in a highly ordered and spontaneous specific form. This process can be carried out, in this case, by OH^- groups adsorbed on the surface of the nanoparticles.

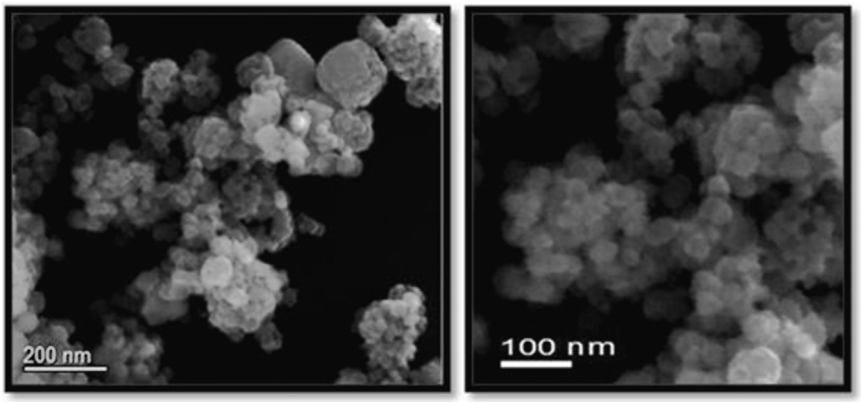

Fig. 5. Scanning Electron Microscopy Images (FE-SEM) of $SrTiO_3$: Eu^{3+}.

This process between particles tends to form three-dimensional architectures, resulting in energy loss. Thus, the process reduces accumulated energies associated with incomplete surfaces at random distances and, by converging, eliminates the mineral-air or mineral-fluid interfaces [32]. The interaction between components of self-organized systems are controlled by hydrogen bonds, Van der Waals forces, and electrostatic or hydrophobic interactions. Both internal interactions and external conditions, such as electrostatic forces, affect the "self-assembly" [33].

Satisfactory conditions for synthesis by the MH method are attributed to the rapid and effective interaction between the electromagnetic radiation and permanent dipole moment of water molecules [34]. In this way, the permanent dipoles of water are induced in solution and can enhance rapid heating of the system because they directly interact with microwaves. This kind of interaction is linked to the capacity for electromagnetic radiation absorption and its effectiveness in converting electromagnetic radiation to thermal energy [35].

If the temperature is high (above 100 °C), the value of the dielectric constant diminishes accompanied by an additional decrease of dielectric loss. Thus, the absorption of electromagnetic radiation reduces very quickly and it is more difficult to heat the solution. Introducing ions into the solution may lead to an increase of dielectric response of the middle of the solution, and may help control reductions in absorption of electromagnetic radiation [36]. KOH is preferred for this role in microwave assisted hydrothermal reactions, because it has advantages over other mineralizer agents. Another benefit of KOH is the high degree of supersaturation during precipitation and, because of its high solubility in water, limited absorption of potassium by the particles [35].

4. Conclusions

In summary, Eu^{3+}-doped $SrTiO_3$ nanoparticles with spherical-like morphology were successfully synthesized by a facile hydrothermal method. The use of microwave energy is able to promote a rapid structural organization of the lattice. The system provided the necessary conditions for rapid crystalline phase formation during MH synthesis under appropriate conditions of temperature and pressure. This process is affected by the action of electromagnetic radiation (2.45 GHz) on solvent polar molecules (water) and generates results that are not achieved by conventional thermal processes. The material exhibits a strong red emission under 393 nm excitation, making this phosphor a promising candidate for application in displays.

Acknowledgments

The Brazilian authors acknowledge the financial support of the Brazilian research financing institutions: FAPESP, CNPq, CAPES and FAPEG (35.0247/2010.2).

References

[1] G. Sreedhara, A. Sivananthama, T. Baskaranb, R. Rajapandianc, S. Vengatesand, L.J. Berchmansa, S.G. Babue, A role of lithiated sarcosine TFSI on the formation of single crystalline $SrTiO_3$ nanocubes via hydrothermal method, Mater. Lett. 133 (2014) 127–131.

[2] Z.Y. Shen, Q.G. Hu, Y.M. Li, Z.M. Wang, W.Q. Luo, Y. Hong, Z.X. Xie, R.H. Liao, Structure and energy storage properties of Ti vacancies charge compensated Re_2O_3-doped $SrTiO_3$ (Re=Pr, Nd, Gd) ceramics, J. Mater. Sci-Mater. El. 24 (2013) 3089–3094.

[3] V.M. Longo, A.T. de Figueiredo, S. de Lazaro, M.F. Gurgel, M.G. S. Costa, C.O. Paiva-Santos, J.A. Varela, E. Longo, V.R. Mastelaro, F.S. De Vicente, A.C. Hernandes, R.W.A. Franco, Structural conditions that leads to photoluminescence emission in $SrTiO_3$: an experimental and theoretical approach, J. Appl. Phys. 104 (2008) 023515.

[4] T. Hara, T. Ishiguro, Oxygen sensitivity of $SrTiO_3$ thin film prepared using atomic layer deposition, Sens. Actuat. B 136 (2009) 489–493.

[5] K.G. Sharma, N.R. Singh, Synthesis and luminescence properties of $CaMO_4$:Dy^{3+} (M=W, Mo) nanoparticles prepared via an ethylene glycol route, J. Lumin. 139 (2013) 98–103.

[6] C. Du, F. Lang, Y. Su, Z. Liu, Using silane coupling agents to prepare raspberry-shaped polyaniline hollow microspheres with tunable nanoshell thickness, J. Colloid Interf. Sci. 394 (2013) 94–99.

[7] O. Chukova, S. Nediko, Z. Moroz, M. Pashkovskyi, Luminescence of the samarium ions doped in the complex oxides with heterovalence substitution, J. Lumin. 102-103 (2003) 498–503.

[8] Z. Yang, Y. Wang, Z. Zhao, Synthesis, structure and photoluminescence properties of fine yellow-orange Ca-α-SiAlON: Eu^{2+} phosphors, J. Alloy Compd. 541 (2012) 70–74.

[9] Y. Jin, Y. Hu, Li. Chen, X. Wang, G. Ju, Z. Mu, Persistent luminescence in Bi^{3+} doped $CaWO_4$ matriz, Radiat. Meas. 51-52 (2013) 18–24.

[10] X. Ma, J. Yin, Q. Zhou, L. Xue, Y. Yan, Effect of Eu doping on structure and electrical properties of lead-free $(Bi_{0.5}Na_{0.5})_{0.94}Ba_{0.06}TiO_3$ ceramics, Ceram. Int. 40 (2014) 7007–7013.

[11] H.K. Yang, H.M. Noh, B.K. Moon, J.H. Jeong, S.S. Yic, Luminescence investigations of Sr_3SiO_5:Eu^{2+} orange–yellow phosphor for UV-based white LED, Ceram. Int. 40 (2014) 12503–12508.

[12] Q. Zhang, Q. Meng, W. Sun,, The concentration dependence of luminescent properties for Eu3+ doped $CaWO_4$ micron spherical phosphors, Opt. Mater. 35 (2013) 915–922.

[13] A. Rothschild, W. Menesklou, H.L. Tuller, E. Ivers-Tiffee, Electronic structure, defect chemistry, and transport properties of $SrTi_{1-x}Fe_xO_{3-y}$ solid solutions, Chem. Mater. 18 (2006) 3651–3659.

[14] L.F. da Silva, M.I.B. Bernardi, L.J.Q. Maia, G.J.M. Frigo, V. R. Mastelaro, Synthesis and thermal decomposition of $SrTi_{1-x}Fe_xO_3$ ($0.0 \le x \le 0.1$) powders obtained by the polymeric precursor method, J. Therm. Anal. Calorim. 97 (2009) 173–177.

[15] A.G.M. Silva, T.S. Rodrigues, A. Dias, H.V. Fajardo, R.F. Gonçalves, M. Godinho, P.A. Robles-Dutenhefner, $Ce_{1-x}Sm_xO_{1.9-\delta}$ nanoparticles obtained by microwave-assisted hydrothermal processing: an efficient application for catalytic oxidation of α-bisabolol, Catal. Sci. Technol 4 (2014) 814–821.

[16] M. Godinho, R.F. Gonçalves, E.R. Leite, C.W. Raubach, N.L.V. Carreño, L.F.D. Probst, E. Longo, H.V. Fajardo, Gadolinium-doped cerium oxide nanorods: novel active catalysts for ethanol reforming, J. Mater. Sci. 45 (2010) 593–598.

[17] A.E. Souza, R.A. Silva, G.T.A. Santos, S.R. Teixeira, S.G. Antonio, M.L. Moreira, D.P. Volanti, E. Longo, Order–disorder degree of self-assembled clusters: influence on photoluminescence emission and morphology of $Ba_xSr_{1-x}TiO_3$ nanocrystals, Chem. Phys. Lett. 514 (2011) 301–306.

[18] M.L. Moreira, V.M. Longo, W. Avansi Jr, M.M. Ferrer, J. Andrés, V.R. Mastelaro, J.A. Varela, E. Longo, Quantum mechanics insight into the microwave nucleation of $SrTiO_3$ nanospheres, J. Phys. Chem. C 116 (2012) 24792–24808.

[19] F.A. Rabuffetti, Hack-Sung Kim, J.A. Enterkin, Y. Wang, C.H. Lanier, L.D. Marks, K.R. Poeppelmeier, P.C. Stair, Synthesis-dependent first-

order raman scattering in $SrTiO_3$ nanocubes at room temperature, Chem. Mater. 20 (2008) 5628–5635.

[20] V.M. Longo, A.T. de Figueiredo, S. de Lázaro, M.F. Gurgel, M.G. S. Costa, C.O. Paiva-Santos, J.A. Varela, E. Longo, V.R. Mastelaro, F.S. DE Vicente, A.C. Hernandes, R.W.A. Franco, Structural conditions that leads to photoluminescence emission in $SrTiO_3$: an experimental and theoretical approach, J. Appl. Phys. 104 (2008) 1–11.

[21] P.F.S. Pereira, A.P. de Moura, I.C. Nogueira, M.V.S. Lima, E. Longo, P.C. de Sousa Filho, O.A. Serra, E.J. Nassar, I.L.V. Rosa, Study of the annealing temperature effect on the structural and luminescent properties of $SrWO_4$:Eu phosphors prepared by a non-hydrolytic sol–gel process, J. Alloy Compd. 526 (2012) 11–21.

[22] L.S. Cavalcante, F.M.C. Batista, M.A.P. Almeida, A.C. Rabelo, I.C. Nogueira, N.C. Batista, J.A. Varela, M.R.M.C. Santos, E. Longo, M. Siu Li, Structural refinement, growth process, photoluminescence and photocatalytic properties of $(Ba_{1-x}Pr_{2x/3})WO_4$ crystals synthesized by the coprecipitation method, RSC Adv. 2 (2012) 6438–6454.

[23] J. Lang, Q. Han, X. Li, S. Xu, J. Yang, L. Yang, Y. Yan, X. Li, Y. Sui, X. Liu, J. Cao, J. Wang, Effect of annealing temperature on the energy transfer in Eu-doped ZnO nanoparticles by chemical precipitation method, J. Mater. Sci-Mater. El. 24 (2013) 4542–4548.

[24] G. Garcıa-Rosales, F. Mercier-Bion, R. Drot, G. Lagarde, J. Roques, E. Simoni, Energy transfer from Tb^{3+} to Eu^{3+} ions sorbed on $SrTiO_3$ surface, J. Lumin. 132 (2012) 1299–1306.

[25] L.F. da Silva, W. Avansi, M.L. Moreira, A. Mesquita, L.J.Q. Maia, J. Andres, E. Longo, V.R. Mastelaro, Relationship between crystal shape, photoluminescence, and local structure in $SrTiO_3$ synthesized by microwave-assisted hydrothermal method (Article ID 890397), J. Nanomater. (2012) 1–6.

[26] T.M. Mazzo, L.M.R. Oliveira, L.R. Macario, W. Avansi Jr., R.S. André, I.L.V. Rosa, J.A. Varela, E. Longo, Photoluminescence properties of $CaTiO_3$:Eu^{3+} nanophosphor obtained by the polymeric precursor method, Mater. Chem. Phys. 145 (2014) 141–150.

[27] S. Ghosh, G.G. Khan, K. Mandal, S. Thapa, P.M.G. Nambissan, Positron annihilation studies of vacancy-type defects and room temperature ferromagnetism in chemically synthesized Li-doped ZnO nanocrystals, J. Alloy Compd. 590 (2014) 396–405.

[28] M. Jiang, X.D. Xue, Z.Q. Chen, Y.D. Liu, H.W. Liang, H.J. Zhang, A. Kawasuso, Defects and acceptor centers in ZnO introduced by C+-implantation, J. Mater. Sci. 49 (2014) 1994–1999.

[29] R.F. Gonçalves, N.L.V. Carreño, M.T. Escote, K.P. Lopes, A. Valentini, E.R. Leite, E. Longo, M.A. Machado, Fotoluminescência e adsorção de CO_2 em nanopartículas de $CaTiO_3$ dopadas com lantânio, Quím. Nova 27 (2004) 862–865.

[30] Q. Zhang, H. Sun, X. Wang, Y. Zhang, X. Li, Strong photoluminescence and piezoelectricity properties in Pr-doped $Ba(Zr_{0.2}Ti_{0.8})O_3$–$(Ba_{0.7}Ca_{0.3})TiO_3$ ceramics: influence of concentration and microstructure, J. Eur. Ceram. Soc. 34 (2014) 1439–1444.

[31] O. Chukova, S. Nedilko, V. Scherbatskyi, Effect of annealing on luminescence properties of the undoped and rare earth doped lead tungstate crystals, Opt. Mater. 34 (12) (2012) 2071–2075.

[32] M. Alfredsson, F. Cora, D.P. Dobson, J. Davy, J.P. Brodholt, S.C. Parker, G.D. Price, Dopant control over the crystal morphology of ceramic materials, Surf. Sci. 601 (2007) 4793–4800.

[33] B.A. Parviz, D. Ryan, G.M. Whitesides, Using self-assembly for the fabrication of nano-scale electronic and photonic devices, IEEE T. Adv. Packag. 26 (2003) 233–241.

[34] G.J. Wilson, A.S. Matijasevich, D.R.G. Mitchell, J.C. Schulz, G.D. Will, Modification of TiO_2 for enhanced surface properties: finite ostwald ripening by a microwave hydrothermal process, Langmuir 22 (2006) 2016–2027.

[35] D. Dallinger, C.O. Kappe, Microwave-assisted synthesis in water as solvent, Chem. Rev. 107 (2007) 2563–2591.

[36] C. Gabriel, S. Gabriel, E.H. Grant, B.S.J. Halstead, D.M.P. Mingos, Dielectric parameters relevant to microwave dielectric heating, Chem. Soc. Rev. 27 (1998) 213–223.